ACTA FACULTATIS
MEDICAE NAISSENSIS

UDC: 615.243.065
DOI: 10.5937/afmnai41-43298

Original article

Design of Vonoprazan Pyrazole Derivatives as Potential Reversible Inhibitors of Gastric Proton Pump: An *In Silico* Molecular Docking Study

Marko Karović[1], Boško Nikolić[2], Nikola Nedeljković[1], Marina Vesović[1], Miloš Nikolić[1]

[1]*University of Kragujevac, Faculty of Medical Sciences, Department of Pharmacy, Kragujevac, Serbia*
[2]*University Clinical Center Kragujevac, Clinic for Gastroenterology and Hepatology, Kragujevac, Serbia*

SUMMARY

Introduction/Aim. Despite the fact that proton pump inhibitors are widely used for the inhibition of gastric acid secretion, recent studies have revealed certain long-term side effects. Due to acidic environment in the stomach, it is challenging to design new competitive inhibitors of gastric proton pump with more potent inhibition of gastric acid secretion to conventional drugs. The aim of this *in silico* study was to assess the potential of designed vonoprazan derivatives to inhibit the gastric proton pump using molecular docking study.

Methods. The distribution-based design of the vonoprazan derivatives was carried out by optimization of the distribution coefficient at physiological pH and pKa values. A molecular docking study was performed using the protein structure of gastric proton pump (PDB ID: 5YLU) in complex with vonoprazan in AutoDock Vina software.

Results. According to the estimated values of docking scores, derivatives 11, 21, and 25 showed the highest binding affinity to gastric proton pump. Compounds 3, 13, 14, 16, 17, 20, 22, and 23 formed the highest number of significant binding interactions with the active site of proton pump.

Conclusion. Based on the obtained binding parameters, it can be concluded that derivatives 14 and 23 achieved the highest number of significant binding interactions (16 and 15, respectively) with concomitant lower values of the docking scores (-9.2 and -9.3 kcal/mol) compared to vonoprazan as a binding control. Based on the binding assessment criteria, these two compounds represent the molecules with the strongest inhibitory potential towards gastric proton pump.

Keywords: **proton pump inhibitors, distribution-based design, vonoprazan derivatives, pyrazole, molecular docking**

Corresponding author:
Miloš Nikolić
e-mail: milos.nikolic@fmn.kg.ac.rs

INTRODUCTION

The most common acid-related gastrointestinal disorders include gastroesophageal reflux disease (GERD), non-erosive reflux disease and peptic ulcer (1, 2). Available therapeutic options are based on preventing parietal cell stimulation by targeting histamine H_2 receptors (3) or on suppressing acid secretion by the inhibition of the gastric proton pump (4).

Although proton pump inhibitors (PPIs) are used as "gold standard" for acid suppression with a side effects incidence of only 1% - 3%, recent studies have revealed certain long-term effects such as renal diseases, fractures and more severe viral diseases including COVID-19 infection (5, 6). Conventional PPIs enter the parietal cell in an inactive form, whereby these protonated prodrugs are accumulated and converted to their active forms. These thiophilic species then form a covalent bond with CYS813 of gastric proton pump, thereby irreversibly inhibiting the enzyme (7, 8). Although PPIs belong to the covalent inhibitors of gastric pump, their ability to inhibit *de novo* synthesis of proton pumps is limited due to their instability and rapid degradation in canaliculus (Figure 1A). Therefore, the clinical use of PPIs requires repeated doses of the drug for several days to reach the maximal inhibitory effect. As a result, PPIs often lead to insufficient control of symptoms during the first three days of therapy and inadequate gastric pH control, especially in some clinical conditions such as control of heartburn and esophageal reflux symptoms at night (9, 10).

These clinical limitations stimulate further development of alternative agents to achieve more potent or at least comparable acid suppression to PPIs.

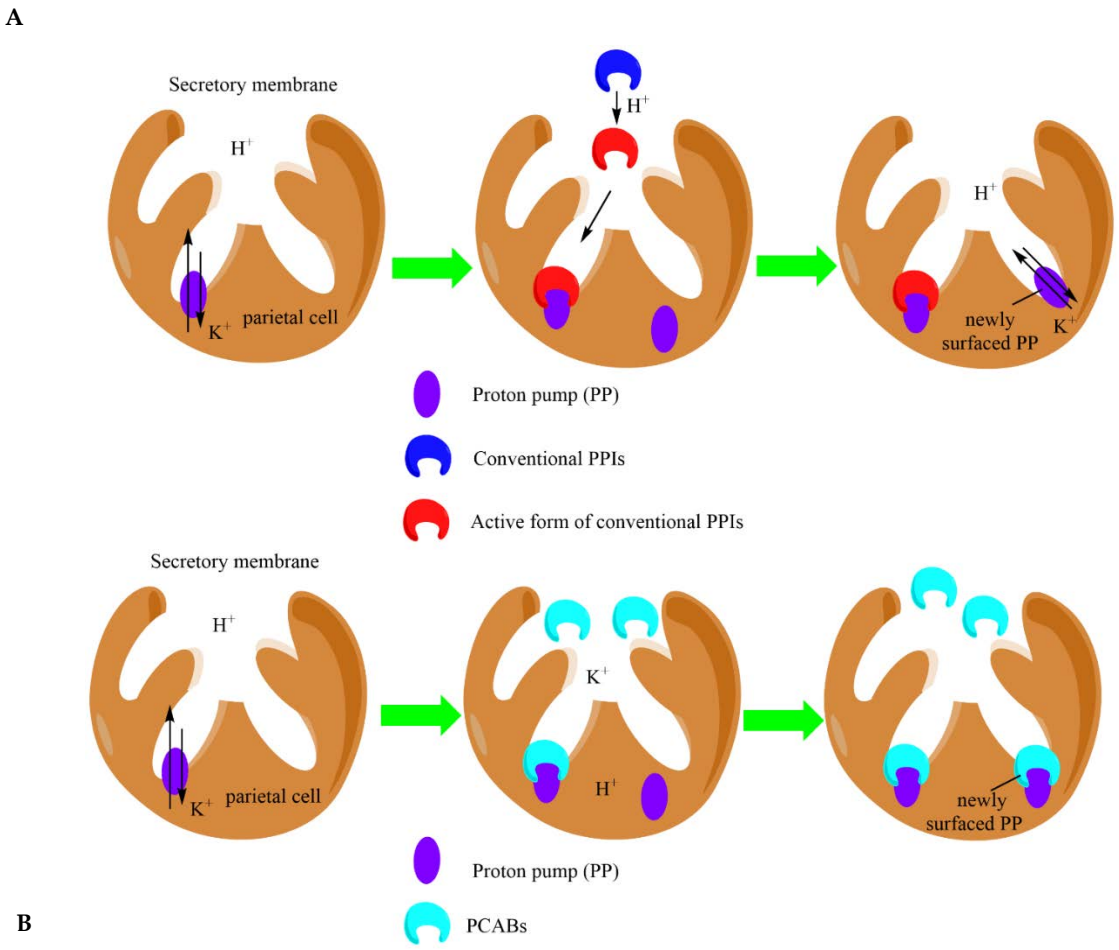

Figure 1. *Schematic representation of the differences in the mechanism of action between conventional proton pump inhibitors - PPIs (A) and K⁺-competitive acid blockers - P-CABs (B).*

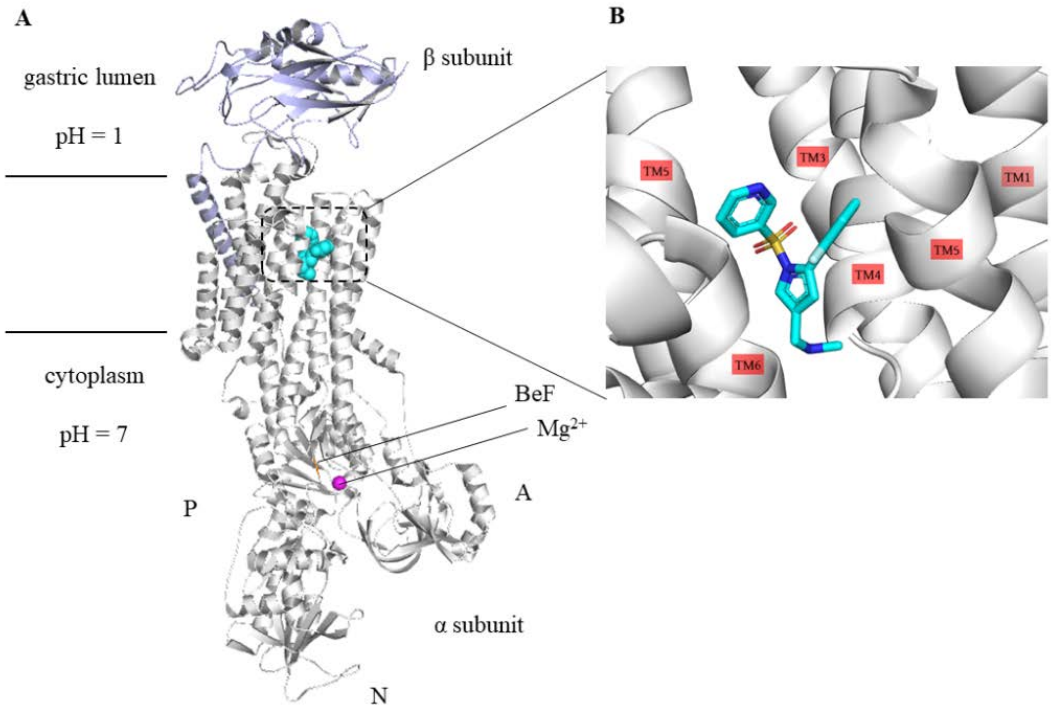

Figure 2. *Overall structure of vonoprazan - H^+, K^+-ATPase complex. (A) Vonoprazan (cyan spheres) is bound to H^+,K^+-ATPase (PDB ID: 5YLU), which consists of the α and β subunits. Within the α subunit, three cytoplasmic domains (A, P, and N domains) and TM helices are shown. Phosphate analogue BeF, and Mg^{2+} ion bound to the P domain are indicated as an orange ribbon and purple sphere. (B) Close-up view of P-CAB-binding site (indicated dotted box in A) for vonoprazan (PDB ID: 5YLU).*

In contrast to PPIs, potassium-competitive acid blockers (P-CABs) enter the parietal cell in an active form (11). After protonation, these molecules accumulate in the canalicular membrane due to their weak base properties (Figure 1B). As a result, P-CABs form non-covalent interactions with gastric proton pump and competitively inhibit this enzyme, thereby achieving fast and steady acid suppression. As reversible competitive inhibitors of gastric proton pump, these drugs are able to inhibit *de novo* synthesis of proton pumps and achieve the full inhibitory effect after the first dose (1, 11).

The acidic environment in the stomach is regulated by the gastric proton pump, also known as H^+, K^+-ATPase. This P2-type ATPase catalyzes H^+ transport from the neutral cytoplasm of the parietal cell into the gastric lumen, followed by ATP hydrolysis. In this way, a very low pH value is maintained in the stomach, which is essential for food digestion (12). Gastric proton pump consists of the catalytic α-subunit and an auxiliary β-subunit. The α-subunit encompass 10 transmembrane (TM) helices in which the cation binding sites and three cytosolic nucleotide (N), phosphorylation (P) and actuator (A) domains are positioned (Figure 2A). In contrast, β-subunit is a glycoprotein with a single TM segment consisting of a small N-terminal cytoplasmic tail and a large C-terminal domain, involved in folding of the complex and membrane integration (13).

Currently, revaprazan (approved in South Korea in 2007) (14), vonoprazan (approved in Japan in 2015) (15, 16), and tegoprazan (approved in South Korea in 2018) (17) are used in clinical practice in Asian countries. According to their half-inhibitory concentration, pyrrole derivative vonoprazan exhibits the highest potency of H^+, K^+-ATPase activity inhibition (0.0015 μM) compared to other P-CABs (12). Its binding site at the gastric proton pump is shown in Figure 2B.

The benefits of vonoprazan usage have been confirmed in GERD, in the eradication of *Helicobacter pylori*, as well as in the treatment of post-endoscopic submucosal dissection ulcers (18). Vonoprazan is a lipophilic weak base and has a pK_a value of 9.1 - 9.3,

which is significantly higher than lansoprazole (pK_a = 3.8), indicating the higher basicity of this compound compared to conventional PPIs (19). In the acidic environment of the stomach, vonoprazan is present predominantly in its ionic form, which has very low cell permeability. Therefore, the drug is rapidly absorbed from the blood into the parietal cell by passive transport, it accumulates there and remains in its ionic form for a long period, even after the nonionic form of vonoprazan has disappeared from the plasma (20).

Nowadays, molecular docking approach has been widely used to identify small molecule inhibitors against various molecular targets. This *in silico* analysis provides a detailed insight into the ligand-receptor interactions and assessment of the binding affinity of various hypothetic, synthetic and naturally occurring molecules (21 - 23).

Design of drugs with improved organ-specific distribution is an important strategy to obtain efficient agents with reduced side effects. Due to unique acidic environment in the stomach, it is challenging to develop new acid suppressants with improved pharmacokinetic and pharmacodynamic properties compared with conventional drugs. Using a distribution-based approach, this study aimed to design vonoprazan pyrazole derivatives by optimizing pK_a and log $D_{7.4}$ values. The potential of designed compounds to inhibit the proton gastric pump was then estimated using an *in silico* molecular docking study.

METHODS

Hardware

Molecular docking study was performed on the Lenovo IdeaPad 3 15ALC6 - 82KU01XGYA, processor 4.00 GHz, memory (RAM) 8.00 GB, 64-bit Operating system, Windows 11 Pro.

Design of tested compounds and *in silico* prediction of physico-chemical properties

Vonoprazan, a proven reversible inhibitor of H^+,K^+-ATPase, served as a designed model for all investigated molecules. Therefore, we conducted the distribution-based design of the vonoprazan pyrazole derivatives to modulate their favorable physico-chemical properties, by optimization of the distribution coefficient at physiological pH (log $D_{7.4}$) and pK_a values. The values of log $D_{7.4}$ and pK_a were calculated using the Marvin Sketch software (24).

SwissADME web server (25) was employed for an *in silico* prediction of physico-chemical properties and lipophilicity parameters of designed compounds. The molecules were then tested for drug-likeness using the Lipinski's (26), Ghose's (27), Veber's (28), Egan's (29), and Muegge's (30) rules. The prediction of passive human gastrointestinal absorption was estimated based on the BOILED-Egg model on the aforementioned web server (31). Gastrointestinal absorption was additionally estimated using the pkCSM online tool predictor (32). After the complete distribution-based design (Scheme 1), twenty-seven compounds (1 - 27) were selected for further binding analysis (Figure 3).

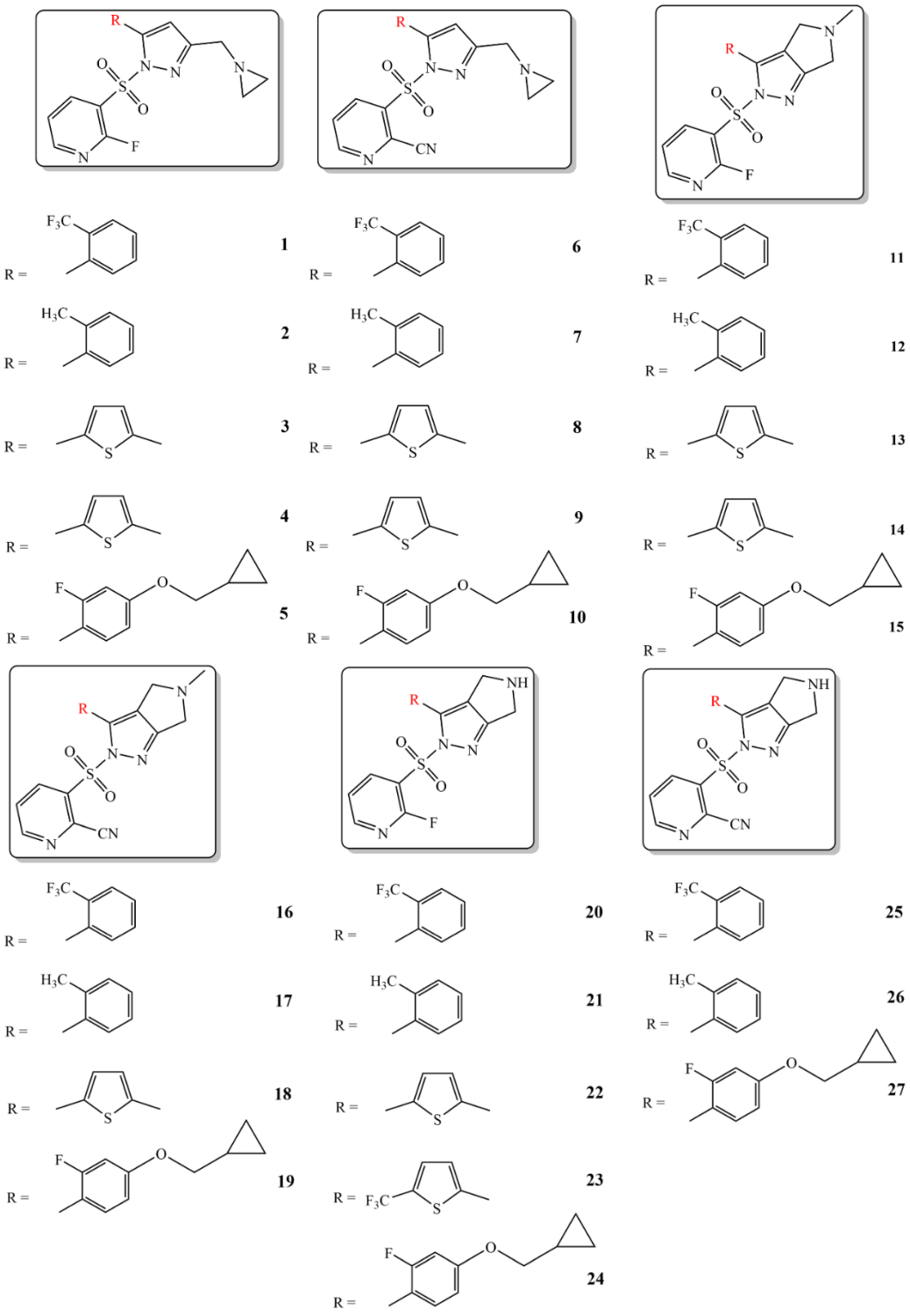

Figure 3. *The chemical structures of the designed compounds*

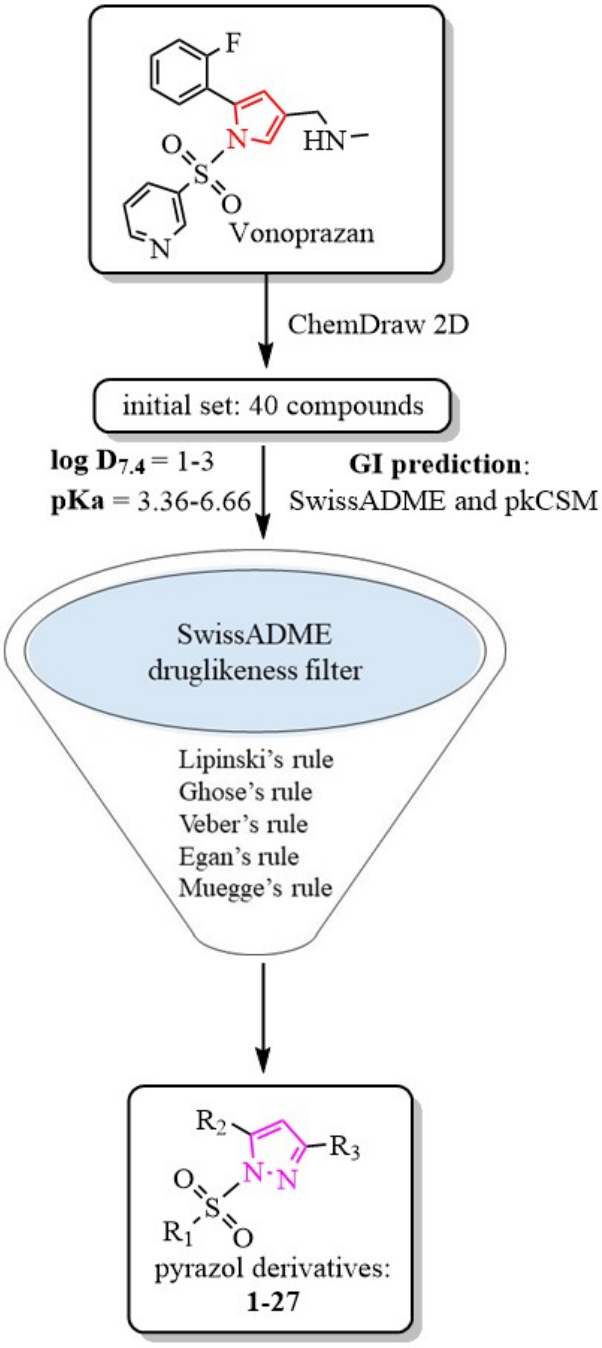

Scheme 1. *Distribution-based design diagram*

Table 1. *Target protein data*

Target	PDB (resolution)	Organism	Co-crystallized ligand	Subunits	Selected chains
H^+,K^+-ATPase	5YLU (2.80 Å)	*Sus scrofa*	vonoprazan	α, β	A

Ligand preparation

All designed molecules were drawn in ChemDraw Ultra 7.0. Their energy optimization was carried out in Chem3D Ultra 7.0 (33) using the AM1 semiempirical quantum method. Molecules were prepared for molecular docking analysis in AutoDockTools 1.5.6 (34), where Gasteiger changes were added and rotatable bonds were defined.

Selection and preparation of receptors

The protein data bank file of H^+, K^+-ATPase (PDB ID: 5YLU) (13) was taken from the Protein data bank (https://www.rcsb.org/) (Table 1). The gastric proton pump was prepared in BIOVIA Discovery Studio Visualizer 2021 (35), thereby docking calculations were performed on chain A of H^+, K^+-ATPase. Preparation of target protein was conducted by adding Kollman charges and hydrogen atoms to protein in AutoDockTools 1.5.6.

Docking methodology

AutoDock Vina software (36) with the default scoring function was utilized for focused semi-flexible docking protocol, thereby protein residues were set conformationally rigid, while selected tested compounds's bonds were defined as rotatable. Based on vonoprazan coordinates, the search area on the target protein was defined as a grid box of 30 x 30 x 30 points. The analogy between the binding mode of vonoprazan and designed molecules was analysed to estimate their inhibitory potential towards H^+, K^+-ATPase. Discovery Studio Visualizer and PyMol (37) were employed for visualization of the best-docked conformation's binding mode. The conformation of designed compounds with the lowest binding energy were modeled into the active sites of the proton gastric pump.

Molecular docking analysis was used to determine the category, type, total number of significant non-covalent binding interactions, and docking scores. The ligand efficiency parameter was calculated using the equation, $LE = \Delta G/N$, where ΔG is a free binding energy (docking score), whereas N is the number of non-hydrogen atoms. The inhibition constants were calculated using the following equation, $\Delta G = RTlnKi$, where T is a temperature of 298 K, R is a gas constant with the value $1.9872036 \cdot 10^{-3}$ kcal $K^{-1}mol^{-1}$, while Ki represents the inhibition constant.

Validation of docking methodology

The accuracy of the molecular docking protocol was confirmed by extracting and re-fitting of the co-crystallized ligand to the native crystal structure. As an indicator of docking validity, the Root-Mean-Square Deviation (RMSD) value was calculated using Discovery Studio Visualizer.

RESULTS

Distribution-based design

The initial set of drawn compounds consists of 40 molecules. The distribution-based design of the drawn compounds was conducted based on the calculation of log $D_{7.4}$ and pK_a values of previously 2D drawn vonoprazan pyrazole derivatives. Thus, all designed molecules have log $D_{7.4}$ values in a range from 1 to 3. The second structural requirement concerned the presence of the ionized form of the molecule in a high percentage at the target site of action. In that sense, the calculated pK_a values of our designed compounds ranged from 3.36 to 6.66, indicating that designed molecules are weak bases. The percentage of ionized form of almost 99% indicates that all designed molecules are in their ionized form in the acidic environment of the stomach. The ionized form of designed molecules is predominantly cationic, thereby the nitrogen atom of the secondary and tertiary amino group is protonated.

Physico-chemical properties, lipophilicity prediction, and drug-likeness analysis of designed compounds

For drug-likeness evaluation, molecular properties and lipophilicity parameters of designed compounds were used. Drug-likeness analysis showed

that 27 designed compounds met the necessary criteria for Lipinski's, Ghose's, Veber's, Egan's, and Muegge's rules. The calculated values of log $D_{7.4}$ and pK_a values along with IUPAC names and percentage of ionized form of selected designed compounds at pH = 1 are shown in Table 2.

Table 2. *IUPAC names and distribution-related parameters of the designed compounds*

Design compound	*IUPAC* name	log $D_{7.4}$	pK_a	Percentage of ionized form at pH=1
1	3-((3-(aziridin-1-ylmethyl)-5-(2-(trifluoromethyl)phenyl)-1*H*-pyrazol-1-yl)sulfonyl)-2-fluoropyridine	2.82	3.58	99.68%
2	3-((3-(aziridin-1-ylmethyl)-5-(o-tolyl)-1*H*-pyrazol-1-yl)sulfonyl)-2-fluoropyridine	2.46	3.63	99.69%
3	3-((3-(aziridin-1-ylmethyl)-5-(5-methylthiophen-2-yl)-1H-pyrazol-1-yl)sulfonyl)-2-fluoropyridine	2.37	3.50	99.64%
4	3-((3-(aziridin-1-ylmethyl)-5-(5-(trifluoromethyl)thiophen-2-yl)-1*H*-pyrazol-1-yl)sulfonyl)-2-fluoropyridine	2.73	3.36	99.53%
5	3-((3-(aziridin-1-ylmethyl)-5-(4-(cyclopropylmethoxy)-2-fluorophenyl)-1*H*-pyrazol-1-yl)sulfonyl)-2-fluoropyridine	2.71	3.53	99.66%
6	3-((3-(aziridin-1-ylmethyl)-5-(2-(trifluoromethyl)phenyl)-1*H*-pyrazol-1-yl)sulfonyl)picolinonitrile	2.53	3.59	99.42%
7	3-((3-(aziridin-1-ylmethyl)-5-(o-tolyl)-1*H*-pyrazol-1-yl)sulfonyl)picolinonitrile	2.16	3.64	99.43%
8	3-((3-(aziridin-1-ylmethyl)-5-(5-methylthiophen-2-yl)-1*H*-pyrazol-1-yl)sulfonyl)picolinonitrile	2.07	3.51	99.38%
9	3-((3-(aziridin-1-ylmethyl)-5-(5-(trifluoromethyl)thiophen-2-yl)-1*H*-pyrazol-1-yl)sulfonyl)picolinonitrile	2.44	3.37	99.27%
10	3-((3-(aziridin-1-ylmethyl)-5-(4-(cyclopropylmethoxy)-2-fluorophenyl)-1*H*-pyrazol-1-yl)sulfonyl)picolinonitrile	2.42	3.54	99.39%
11	2-((2-fluoropyridin-3-yl)sulfonyl)-5-methyl-3-(2-(trifluoromethyl)phenyl)-2,4,5,6-tetrahydropyrrolo[3,4-c]pyrazole	2.74	3.96	99.87%
12	2-((2-fluoropyridin-3-yl)sulfonyl)-5-methyl-3-(o-tolyl)-2,4,5,6-tetrahydropyrrolo[3,4-c]pyrazole	2.38	4.07	99.89%
13	2-((2-fluoropyridin-3-yl)sulfonyl)-5-methyl-3-(5-methylthiophen-2-yl)-2,4,5,6-tetrahydropyrrolo[3,4-c]pyrazole	2.29	3.91	99.86%
14	2-((2-fluoropyridin-3-yl)sulfonyl)-5-methyl-3-(5-(trifluoromethyl)thiophen-2-yl)-2,4,5,6-tetrahydropyrrolo[3,4-c]pyrazole	2.65	3.66	99.77%
15	3-(4-(cyclopropylmethoxy)-2-fluorophenyl)-2-((2-fluoropyridin-3-yl)sulfonyl)-5-methyl-2,4,5,6-tetrahydropyrrolo[3,4-c]pyrazole	2.63	3.65	99.75%
16	3-((5-methyl-3-(2-(trifluoromethyl)phenyl)-5,6-dihydropyrrolo[3,4-c]pyrazol-2(4*H*)-yl)sulfonyl)picolinonitrile	2.45	3.97	99.60%
17	3-((5-methyl-3-(o-tolyl)-5,6-dihydropyrrolo[3,4-c]pyrazol-2(4*H*)-yl)sulfonyl)picolinonitrile	2.09	4.08	99.62%
18	3-((5-methyl-3-(5-methylthiophen-2-yl)-5,6-dihydropyrrolo[3,4-c]pyrazol-2(4*H*)-yl)sulfonyl)picolinonitrile	2.00	3.92	99.60%
19	3-((3-(4-(cyclopropylmethoxy)-2-fluorophenyl)-5-methyl-5,6-dihydropyrrolo[3,4-c]pyrazol-2(4*H*)-yl)sulfonyl)picolinonitrile	2.34	3.65	99.49%
20	2-((2-fluoropyridin-3-yl)sulfonyl)-3-(2-(trifluoromethyl)phenyl)-2,4,5,6-tetrahydropyrrolo[3,4-c]pyrazole	2.29	6.65	99.98%
21	2-((2-fluoropyridin-3-yl)sulfonyl)-3-(o-tolyl)-2,4,5,6-tetrahydropyrrolo[3,4-c]pyrazole	1.93	6.66	99.97%
22	2-((2-fluoropyridin-3-yl)sulfonyl)-3-(5-methylthiophen-2-yl)-2,4,5,6-tetrahydropyrrolo[3,4-c]pyrazole	1.84	6.63	99.98%
23	2-((2-fluoropyridin-3-yl)sulfonyl)-3-(5-(trifluoromethyl)thiophen-2-yl)-2,4,5,6-tetrahydropyrrolo[3,4-c]pyrazole	2.20	6.62	99.99%
24	3-(4-(cyclopropylmethoxy)-2-fluorophenyl)-2-((2-fluoropyridin-3-yl)sulfonyl)-2,4,5,6-tetrahydropyrrolo[3,4-c]pyrazole	2.18	6.64	99.98%

25	3-((3-(2-(trifluoromethyl)phenyl)-5,6-dihydropyrrolo[3,4-c]pyrazol-2(4*H*)-yl)sulfonyl)picolinonitrile	2.00	6.65	99.69%
26	3-((3-(o-tolyl)-5,6-dihydropyrrolo[3,4-c]pyrazol-2(4*H*)-yl)sulfonyl)picolinonitrile	1.63	6.66	99.68%
27	3-((3-(4-(cyclopropylmethoxy)-2-fluorophenyl)-5,6-dihydropyrrolo[3,4-c]pyrazol-2(4*H*)-yl)sulfonyl)picolinonitrile	1.89	6.64	99.69%

Table 3. *Predicted physico-chemical properties of designed compounds*

Designed compound	Molecular weight (g/mol)	Number of heavy atoms	Number of aromatic heavy atoms	Number of rotatable bonds	Number of H-bond acceptors	Number of H-bond donors	Molar refractivity	TPSA (Å²)
1	426.39	29	17	6	9	0	98.76	76.24
2	372.42	26	17	5	6	0	98.73	76.24
3	378.44	25	16	5	6	0	96.61	104.48
4	432.42	28	16	6	9	0	96.64	104.48
5	446.47	31	17	8	8	0	112.52	85.47
6	433.41	30	17	6	9	0	103.52	100.03
7	379.44	27	17	5	6	0	103.49	100.03
8	378.44	25	16	5	6	0	96.61	104.48
9	432.42	28	16	6	9	0	96.64	104.48
10	453.49	32	17	8	8	0	117.28	109.26
11	426.39	29	17	4	9	0	98.92	76.47
12	372.42	26	17	3	6	0	98.89	76.47
13	378.44	25	16	3	6	0	96.77	104.71
14	432.42	28	16	4	9	0	96.8	104.71
15	446.47	31	17	6	8	0	112.68	85.7
16	433.41	30	17	4	9	0	103.68	100.26
17	379.44	27	17	3	6	0	103.64	100.26
18	385.46	26	16	3	6	0	101.52	128.5
19	453.49	32	17	6	8	0	117.44	109.49
20	412.36	28	17	4	9	1	94.02	85.26
21	358.39	25	17	3	6	1	93.99	85.26
22	364.42	24	16	3	6	1	91.86	113.5
23	418.39	27	16	4	9	1	91.9	113.5
24	432.44	30	17	6	8	1	107.78	94.49
25	419.38	29	17	4	9	1	98.78	109.05
26	365.41	26	17	3	6	1	98.74	109.05
27	439.46	31	17	6	8	1	112.53	118.28

Table 4. *Predicted partition coefficients of designed compounds*

Designed compound	Log P (iLOGP)	Log P (XLOGP3)	Log P (MLOGP)	Log P (SILICOS-IT)
1	2.74	3.02	3.26	2.92
2	2.61	2.50	2.65	2.37
3	2.57	2.25	2.21	3.02
4	2.25	2.77	2.83	3.58
5	2.79	2.95	3.17	3.14
6	2.29	2.64	2.23	2.53
7	2.14	2.12	1.62	1.97
8	2.57	2.25	2.21	3.02
9	2.25	2.77	2.83	3.58
10	3.23	2.57	2.15	2.76
11	3.03	2.82	3.26	2.82
12	2.45	2.30	2.65	2.27
13	2.48	2.05	2.21	2.92
14	2.46	2.57	2.83	3.48
15	3.17	2.75	3.17	3.04
16	2.54	2.43	2.23	2.43
17	2.30	1.91	1.62	1.88
18	2.91	1.67	1.19	2.52
19	3.00	2.37	2.15	2.66
20	2.21	2.35	3.03	2.88
21	2.19	1.83	2.41	2.34
22	2.04	1.58	1.96	3.00
23	1.72	2.10	2.60	3.55
24	2.66	2.28	2.95	3.10
25	2.14	1.97	2.01	2.49
26	1.90	1.45	1.39	1.94
27	2.59	1.90	1.93	2.71

The physico-chemical properties of the designed compounds obtained in SwissADME predictor are shown in Table 3.

The predicted partition coefficients calculated by different methods are shown in Table 4.

The values of partition coefficients show that tested molecules have optimal liposolubility, with all calculated values of log P greater than zero.

Prediction of passive human gastrointestinal absorption

The BOILED-Egg diagram (Figure 4) displays that all points representing the selected molecules lie in the white ellipse, indicating that these compounds have a high probability of good intestinal absorption. The blue and red dots indicate that the selected compounds are substrates (PGP+) or non-substrates (PGP-) of the P-glycoprotein.

The predictions obtained in pkCSM online server shows that designed compounds have a percentage of gastrointestinal absorption ranging from 91.377 to 99.351% (Table 5).

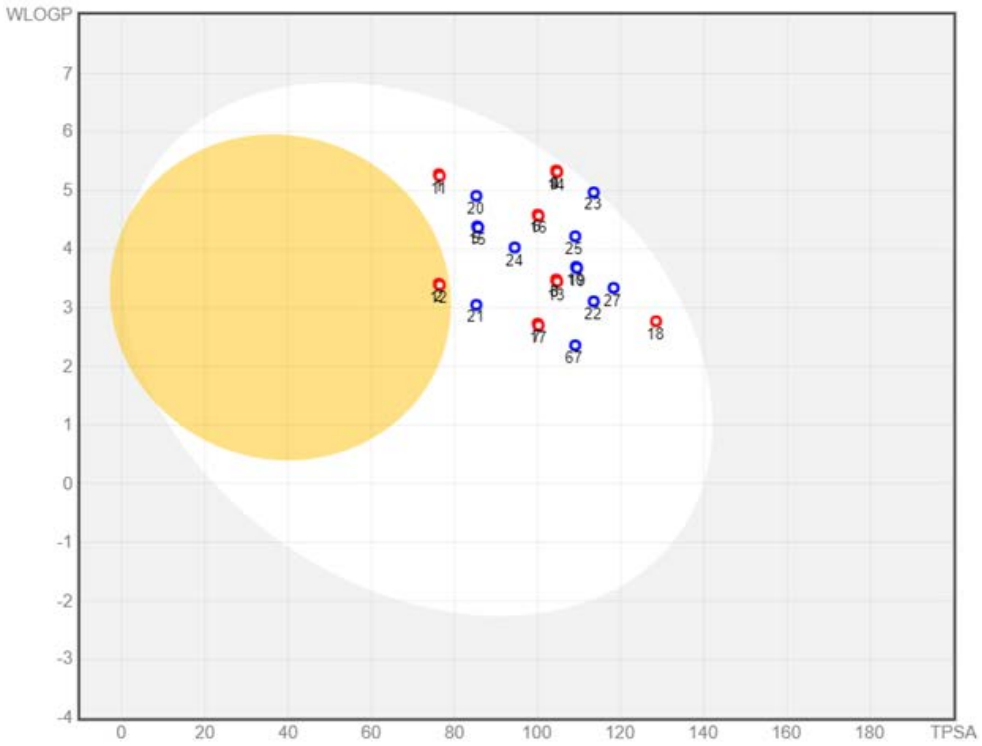

Figure 4. *The BOILED-Egg plot of designed compounds. Yellow eclipse indicates blood brain barrier penetration, white eclipse represents human intestinal absorption, whereas blue and red dots indicate the probability of the tested compounds acting as a substrate (PGP+) or non-substrate (PGP-) of the P-glycoprotein.*

Table 5. *Predicted percentages of intestinal absorption of designed compounds*

Designed compound	Intestinal absorption (%)	Designed compound	Intestinal absorption (%)
1	93.303	15	95.194
2	96.465	16	94.054
3	95.644	17	92.246
4	92.767	18	92.652
5	95.681	19	98.447
6	95.037	20	94.098
7	93.267	21	96.357
8	95.644	22	94.047
9	92.767	23	91.587
10	99.351	24	95.404
11	93.888	25	93.335
12	96.147	26	91.527
13	93.837	27	97.728
14	91.377		

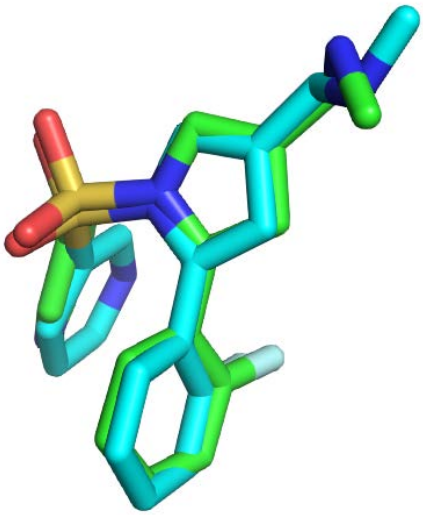

Figure 5. *RMSD of the superimposed crystallographic and re-docked conformation of vonoprazan. The crystallographic pose of vonoprazan is highlighted in green, while the re-docked conformation is highlighted in cyan.*

Validation of molecular docking protocol

The RMSD value was calculated by overlapping the native binding pose of vonoprazan from the crystal structure and its re-docked binding conformation obtained by molecular docking study in Discovery Studio Visualizer (Figure 5). Considering that the obtained RMSD value (1.1502 Å) was less than 2 Å, we can assume that molecular docking protocol was properly performed.

Binding analysis

In this *in silico* study, 27 previously designed compounds were modeled into the active site of the H^+, K^+-ATPase. In the interpretation of the molecular docking results, we considered the significant binding interactions to be those interactions achieved by the co-crystallized ligand during its molecular fitting into the active site of the proton pump. The residues that form significant binding interactions with vonoprazan in the active site of H^+, K^+-ATPase are shown in Figure 6.

The category, type, total number of significant binding non-covalent interactions, docking scores of the best fitted ligand's poses, ligand efficiency, and inhibition constants are the main binding parameters of the tested compounds used to determine their binding analogy with the vonoprazan binding mode.

Considering only the docking score, three compounds with the lowest binding energy were singled out. Compounds 11, 21, and 25 achieved the lowest binding energy of -9.7, -9.8, and -10.2 kcal/mol, with calculated inhibition constants of 0.08, 0.06, and 0.03 μM, respectively, during molecular fitting into the active site of H^+, K^+-ATPase (Figure 7A-C). Otherwise, the calculated inhibition constants for all designed compounds were in the range from 0.03 to 3.71 μM. For comparison, vonoprazan achieved a free binding energy value of -9.0 kcal/mol and inhibition constant of 0.249 μM. The lowest binding energy of ligand to protein per atom was observed for compounds 21 and 22 (-0.39 and -0.38 kcal/mol, respectively).

On the other hand, compounds 3, 13, 14, 16, 17, 20, 22 and 23 formed the highest number of the significant binding interactions in the active site of the gastric proton pump (Table 6).

A two-dimensional and three-dimensional view of the significant binding interactions achieved by these compounds in the active site of the gastric proton pump is shown in Figures 8 - 15 (A and B).

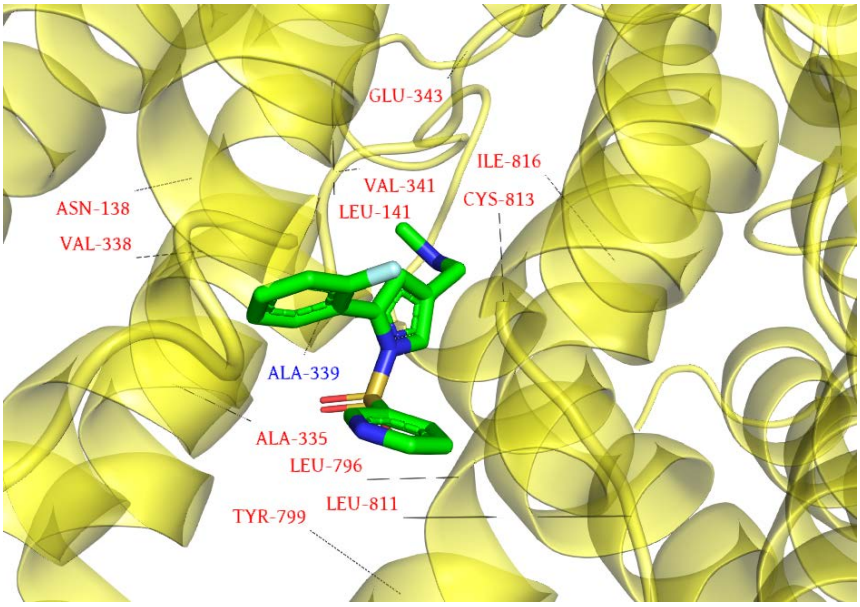

Figure 6. *Close-up view of the vonoprazan binding site. The amino acid residues that form significant binding interactions with vonoprazan in the active site of H^+, K^+-ATPase are shown. Hydrophobic residues are highlighted in red, while residues forming hydrogen bonds are colored in blue.*

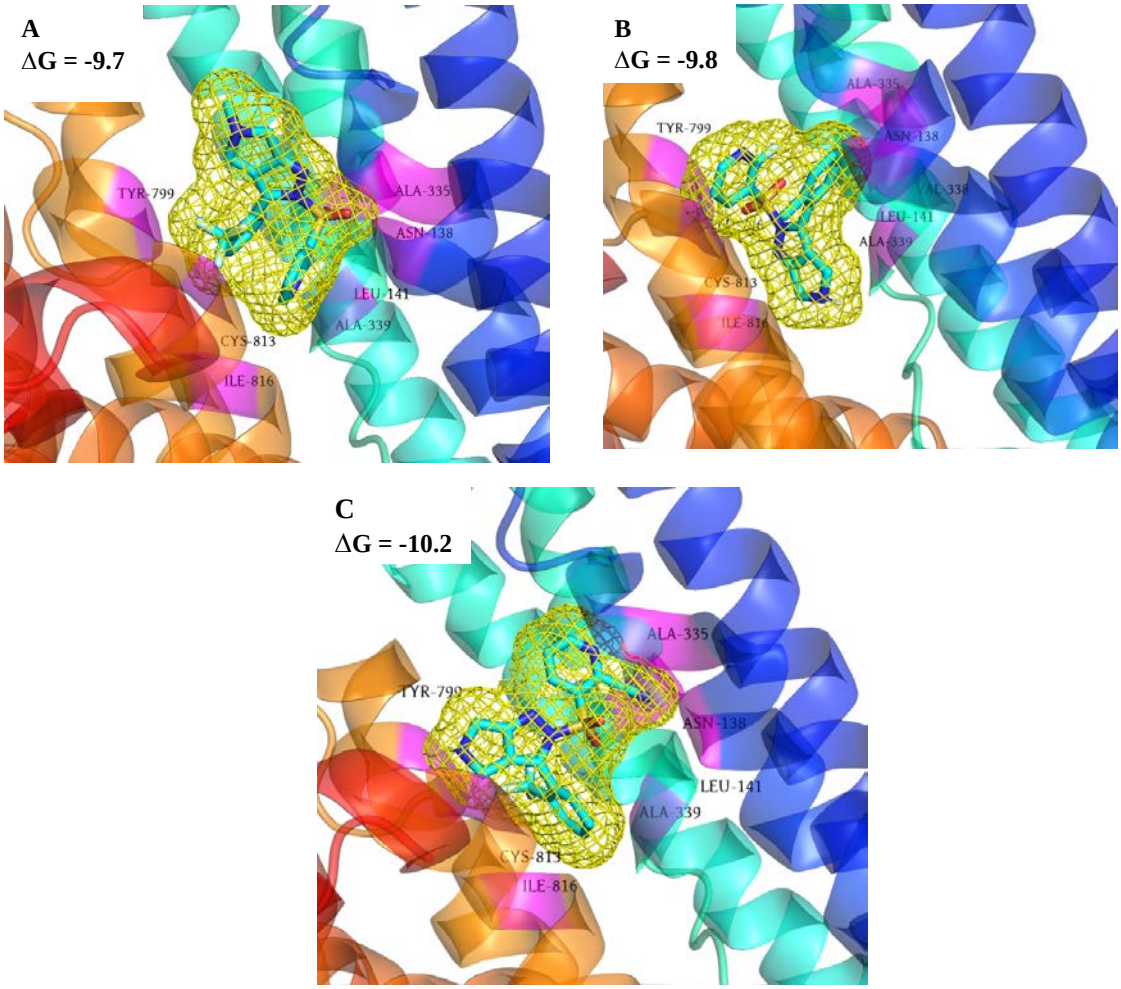

Figure 7. *The molecular docking of the compounds 11 (A), 21 (B) and 25 (C) into the active site of the gastric proton pump. Docking visualization is represented by mesh representation (colored yellow) of the best modeled conformation (colored cyan) of compound 11 (-9.7 kcal/mol), 21 (-9.8 kcal/mol), and 25 (-10.2 kcal/mol) in the binding pocket of the protein (colored magenta).*

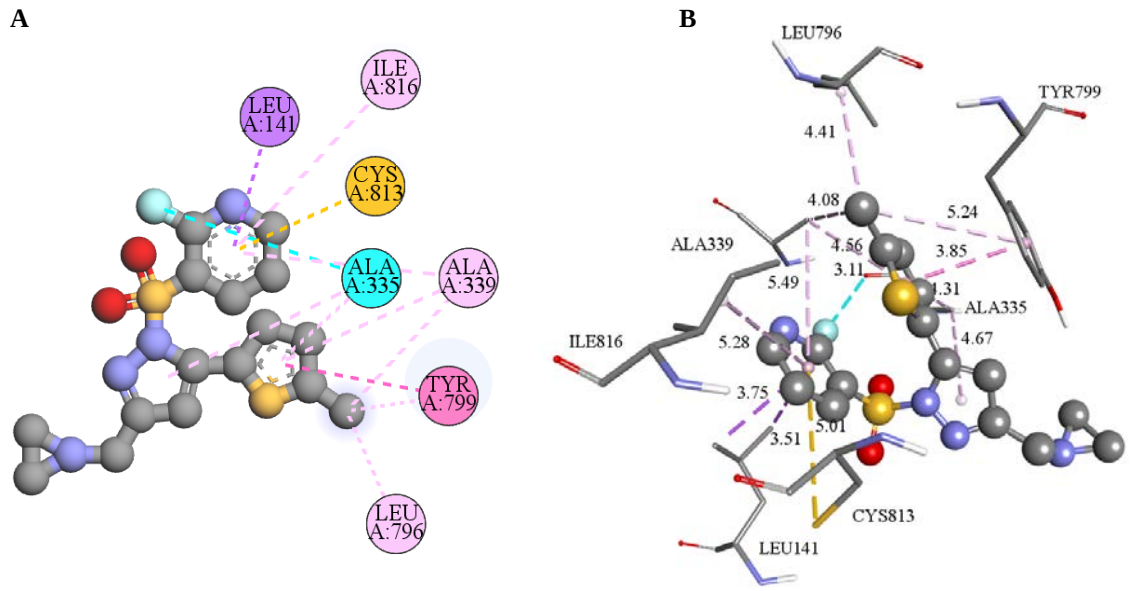

Figure 8. *Designed compound 3 modeled into the active site of the gastric proton pump. (A) Two-dimensional and (B) three-dimensional representation of significant binding interactions formed by compound 3. π-σ interactions (purple dotted lines), π-sulfur interactions (orange dotted lines), hydrophobic interactions (rose pink and magenta dotted lines), and halogen interactions (cyan dotted lines) are shown.*

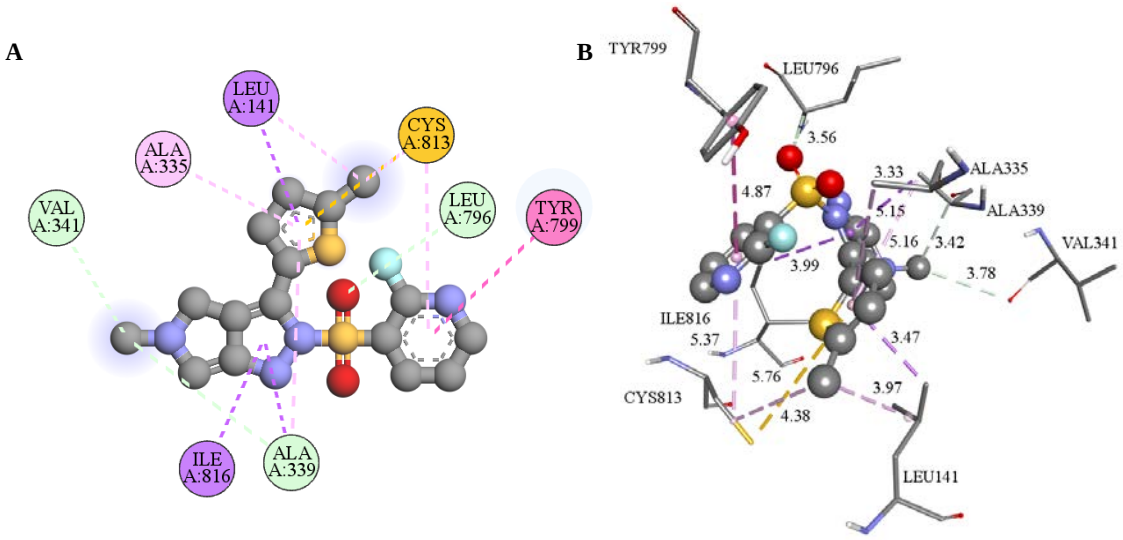

Figure 9. *Designed compound 13 modeled into the active site of the gastric proton pump. (A) Two-dimensional and (B) three-dimensional representation of significant binding interactions formed by compound 13. Carbon-hydrogen bonds (pale green dotted lines), π-σ interactions (purple dotted lines), π-sulfur interactions (orange dotted lines), and hydrophobic interactions (rose pink and magenta dotted lines) are shown.*

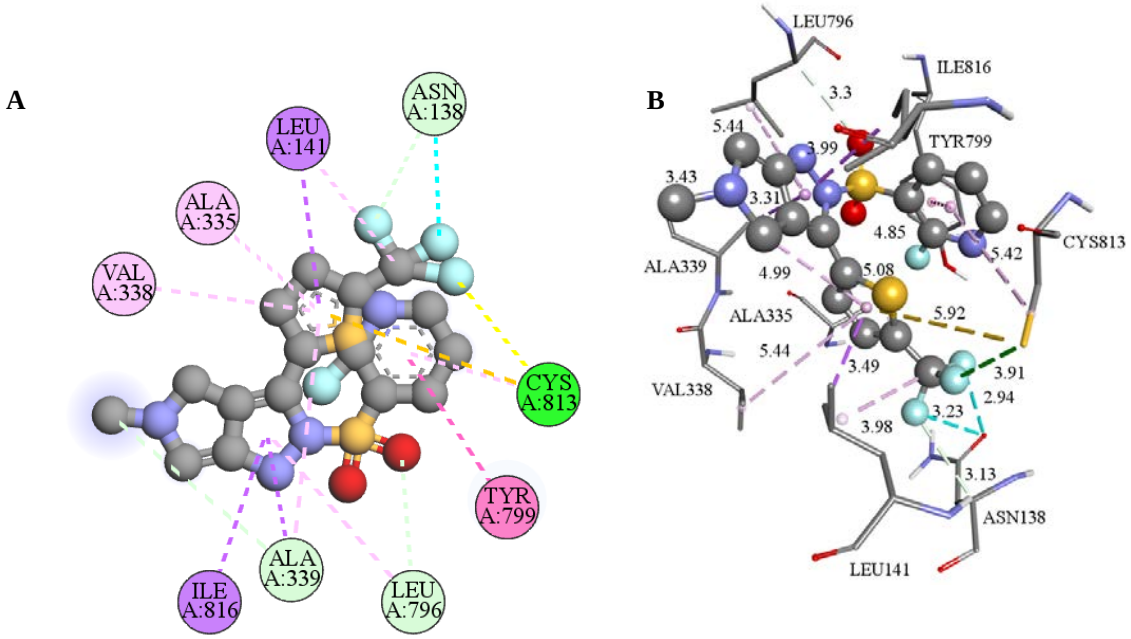

Figure 10. *Designed compound 14 modeled into the active site of gastric proton pump. (A) Two-dimensional and (B) three-dimensional representation of significant binding interactions formed by compound 14. The conventional hydrogen bonds (green dotted lines), carbon-hydrogen bonds (pale green dotted lines), π-σ interactions (purple dotted lines), and hydrophobic interactions (rose pink and magenta dotted lines) are shown.*

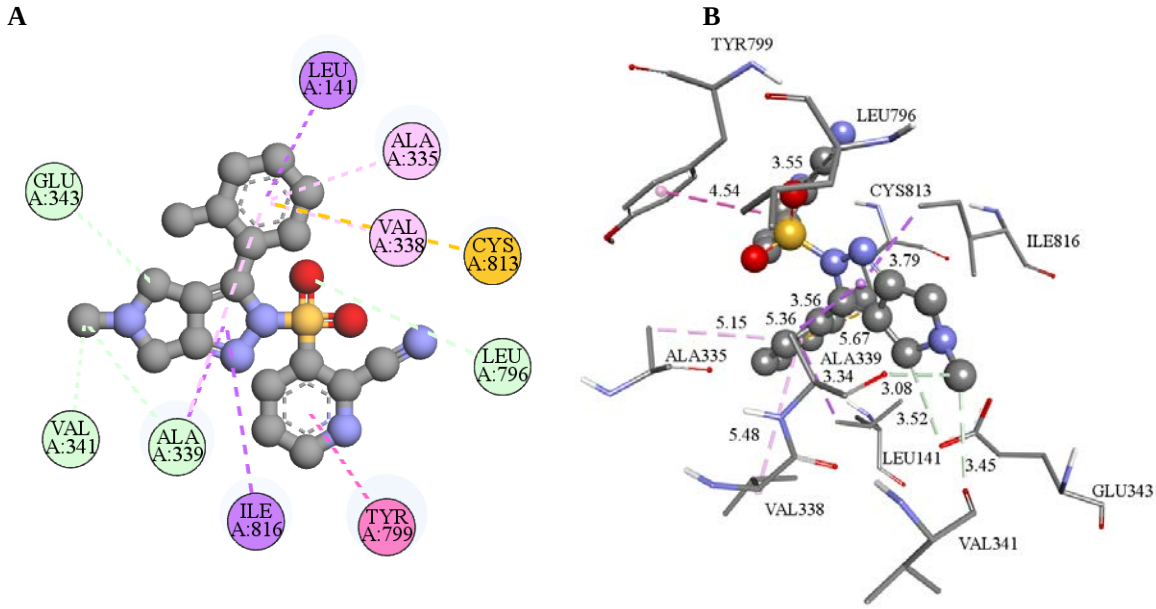

Figure 11. *Designed compound 16 modeled into the active site of gastric proton pump. (A) Two-dimensional and (B) three-dimensional representation of significant binding interactions formed by compound 16. The carbon-hydrogen bonds (pale green dotted lines), π-σ interactions (purple dotted lines), and hydrophobic interactions (rose pink and magenta dotted lines) are shown.*

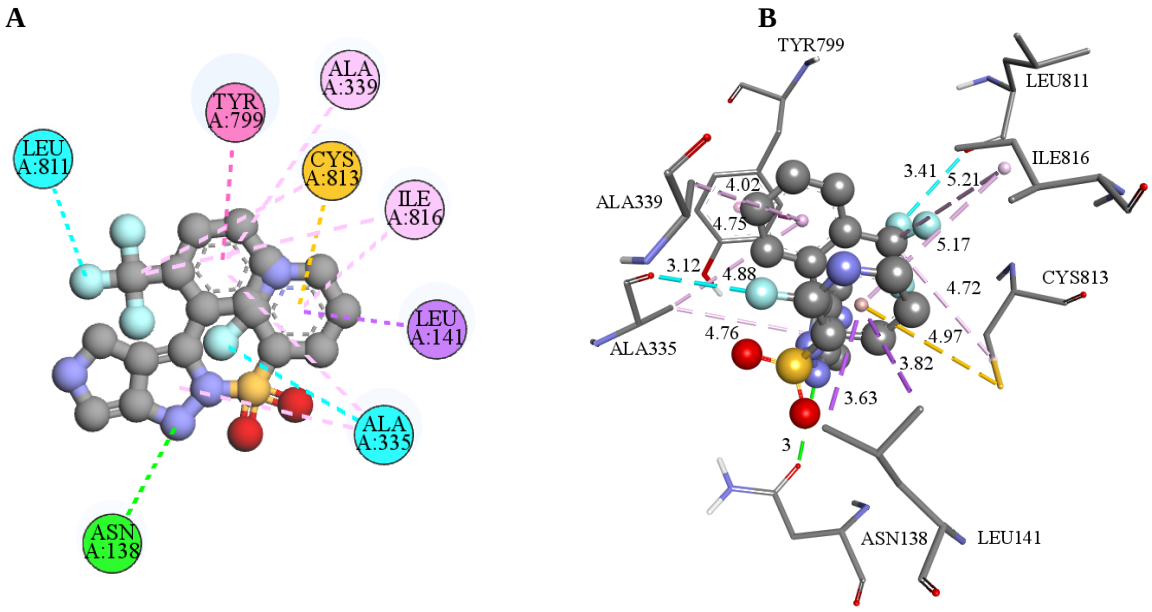

Figure 12. *Designed compound 17 modeled into the active site of gastric proton pump. (A) Two-dimensional and (B) three-dimensional representation of significant binding interactions formed by compound 17. The carbon-hydrogen bonds (pale green dotted lines), π-σ interactions (purple dotted lines), π-sulfur interactions (orange dotted lines), and hydrophobic interactions (rose pink and magenta dotted lines) are shown.*

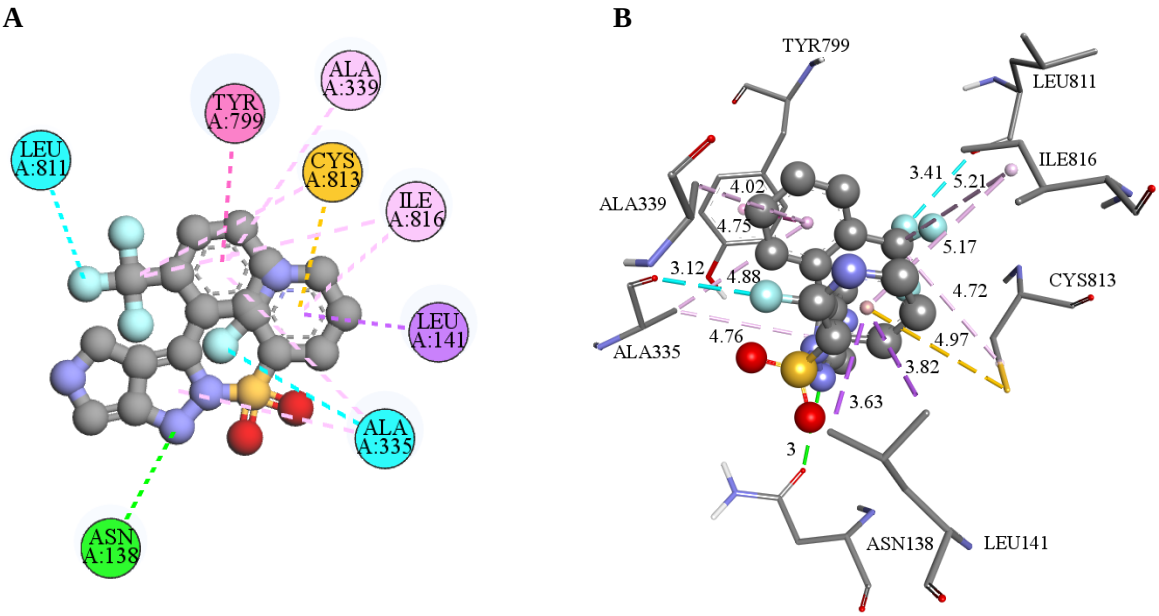

Figure 13. *Designed compound 20 modeled into the active site of gastric proton pump. (A) Two-dimensional and (B) three-dimensional representation of significant binding interactions formed by compound 20. The conventional hydrogen bonds (green dotted lines), π-σ interactions (purple dotted lines), π-sulfur interactions (orange dotted lines), hydrophobic interactions (rose pink and magenta dotted lines), and halogen interactions (cyan dotted lines) are shown.*

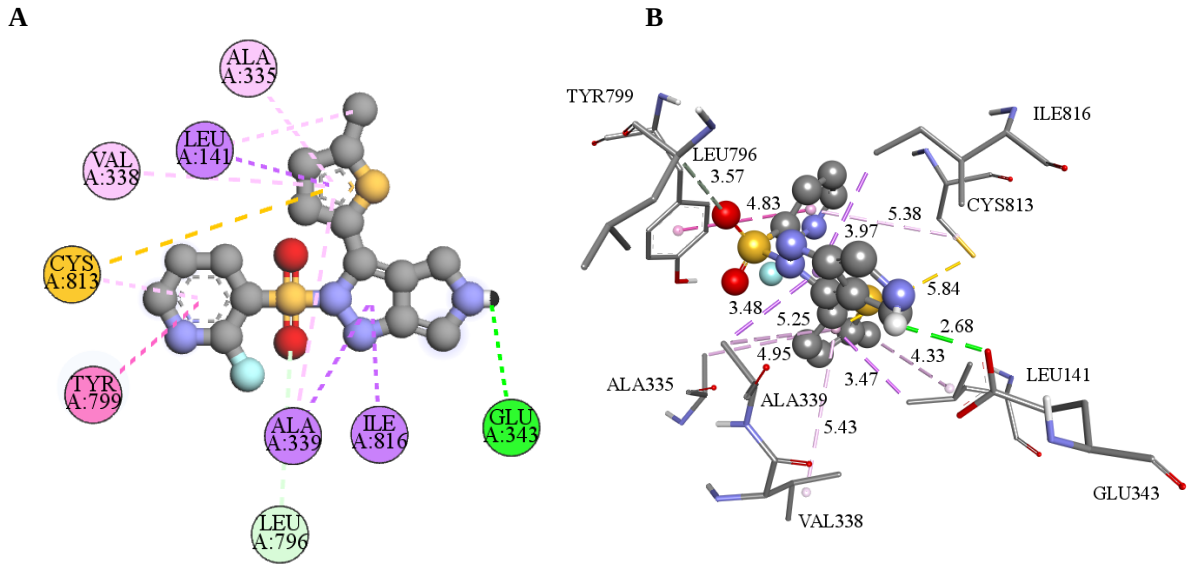

Figure 14. *Designed compound 22 modeled into the active site of gastric proton pump. (A) Two-dimensional and (B) three-dimensional representation of significant binding interactions formed by compound 22. The conventional hydrogen bonds (green dotted lines), carbon-hydrogen bonds (pale green dotted lines), π-σ interactions (purple dotted lines), π-sulfur interactions (orange dotted lines), and hydrophobic interactions (rose pink and magenta dotted lines) are shown.*

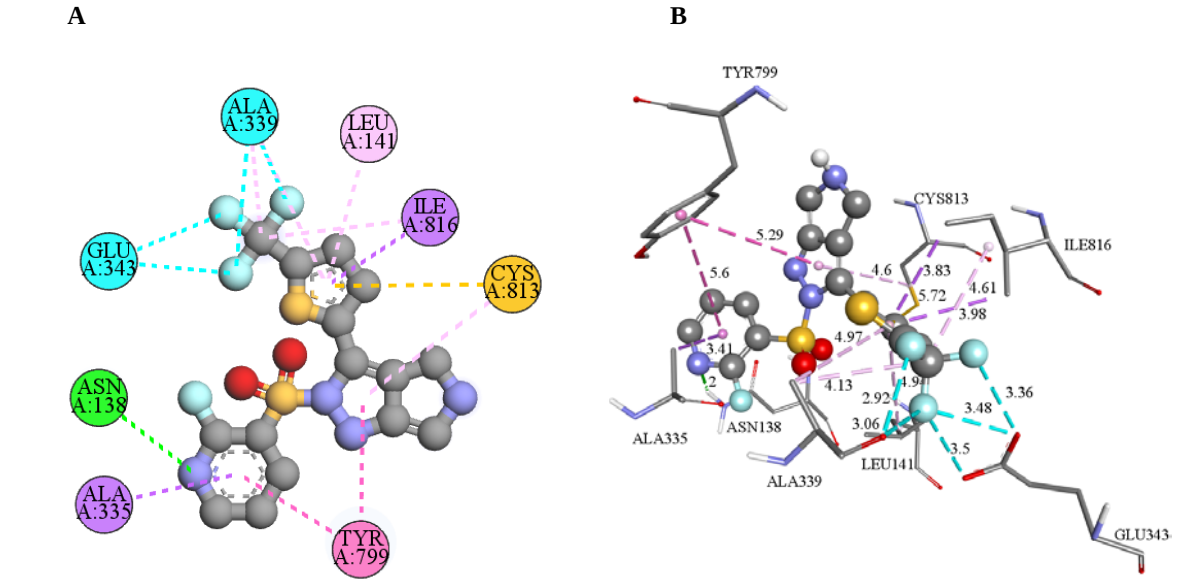

Figure 15. *Designed compound 23 modeled into the active site of gastric proton pump. (A) Two-dimensional and (B) three-dimensional representation of significant binding interactions formed by compound 23. The conventional hydrogen bonds (green dotted lines), π-σ interactions (purple dotted lines), π-sulfur interactions (orange dotted lines), hydrophobic interactions (rose pink and magenta dotted lines), and halogen interactions (cyan dotted lines) are shown.*

Table 6. *The main molecular docking parameters of the designed compounds*

Ligand	Significant binding interactions (category)	Residues and type of interaction	Number of significant binding interaction	ΔG_{bind} (kcal/mol)	LE* (kcal/mol)	K_i (μM)
1	Hydrophobic interactions	Leu141(π-σ); Ala335 (π-alkyl); Ala335 (π-alkyl); Ala339 (π-alkyl); Tyr799 (π-alkyl); Tyr799 (π-π stacked); Cys813 (alkyl); Cys813 (π-sulfur); Ile816 (π-alkyl); Ile816 (π-alkyl);	10	-9.1	-0.31	0.21
2	Hydrophobic interactions	Leu141(π-σ); Ala335 (π-alkyl) Ala335 (π-alkyl); Ala339 (π-alkyl) Ala339 (π-alkyl); Tyr799 (π-π stacked) Cys813 (π-sulfur); Ile816 (π-alkyl);	8	-8.7	-0.33	0.41
3	Hydrophobic interactions	Leu141(π-σ); Ala335 (π-alkyl); Ala335 (π-alkyl); Ala335 (halogen); Ala339 (π-alkyl); Ala339 (π-alkyl); Ala339 (alkyl); Leu796 (alkyl); Tyr799 (π-π stacked); Tyr799 (π-alkyl); Cys813 (π-sulfur); Ile816 (π-alkyl);	12	-7.9	-0.33	1.60
4	Hydrophobic interactions	Asn138 (halogen); Ala335 (π-σ); Ala339 (halogen); Ala339 (π-alkyl); Ala339 (alkyl); Tyr799 (π-π T-shaped); Cys813 (π-alkyl); Ile816 (π-alkyl); Ile816 (alkyl);	11	-8.8	-0.31	0.35
	Hydrogen bonds	Asn138 (conventional) Ala339 (carbon-hydrogen)				
5	Hydrophobic interactions	Asn138 (halogen); Ala335 (π-alkyl); Ala339 (π-alkyl); Ala339 (alkyl); Ile816 (π-alkyl); Tyr799 (π-π T-shaped);	7	-8.2	-0.26	0.96
	Hydrogen bonds	Tyr799 (conventional)				
6	Hydrophobic interactions	Ala335 (π-σ); Ala339 (π-alkyl); Leu796 (alkyl); Tyr799 (π-alkyl); Cys813 (π-alkyl); Cys813 (π- sulfur); Ile816 (π-σ);	9	-9.5	-0.30	0.11
	Hydrogen bonds	Asn138 (conventional) Leu796 (carbon-hydrogen)				
7	Hydrophobic interactions	Leu141(π-σ); Leu141(alkyl); Ala335 (π-alkyl); Ala335 (alkyl); Val338 (alkyl); Ala339 (π-alkyl); Tyr799 (π-π stacked); Tyr799 (π- sulfur); Cys813 (π-alkyl); Ile816 (π-alkyl);	10	-8.7	-0.32	0.41
	Hydrogen bonds	Glu343 (carbon-hydrogen)				
8	Hydrophobic interactions	Leu141(π-σ); Leu141(alkyl); Ala335 (alkyl); Ala335 (π-alkyl); Val338 (alkyl); Ala339 (π-alkyl); Leu796 (π-alkyl); Tyr799 (π-π T-shaped); Cys813 ((π-alkyl); Ile816 (π-alkyl);	11	-7.4	-0.28	3.71
	Hydrogen bonds	Cys813 (carbon-hydrogen)				
9	Hydrophobic interactions	Ala335 (π-σ); Ala339 (π-alkyl); Ala339 (alkyl); Ala339 (halogen); Ala339 (halogen); Cys813 (π-alkyl); Ile816 (π-alkyl); Ile816 (alkyl);	9	-8.9	-0.31	0.29
	Hydrogen bonds	Asn138 (conventional)				
10	Hydrophobic interactions	Ala335 (π-σ); Ala339 (π-alkyl); Tyr799 (π-π T-shaped); Cys813 (π-alkyl); Ile816 (π-alkyl);	6	-8.6	-0.27	0.49

	Hydrogen bonds	Asn138 (conventional)				
11	Hydrophobic interactions	Leu141 (π-σ); Ala335 (π-alkyl); Ala335 (π-alkyl); Ala335 (halogen); Ala339 (π-alkyl); Tyr799 (π-π stacked); Cys813 (π-sulfur); Ile816 (π-alkyl); Ile816 (alkyl);	10	-9.7	-0.33	0.08
	Hydrogen bonds	Asn138 (conventional)				
12	Hydrophobic interactions	Leu141(π-σ); Ala335 (π-alkyl); Ala335 (halogen); Ala339 (π-alkyl); Ala339 (π-alkyl); Tyr799 (π-π stacked); Cys813 (π-sulfur); Ile816 (π-alkyl);	9	-9.0	-0.35	0.25
	Hydrogen bonds	Asn138 (conventional)				
13	Hydrophobic interactions	Leu141 (π-σ); Leu141 (alkyl); Ala335 (π-alkyl); Ala339 (π-σ); Ala339 (π-alkyl); Tyr799 (π-π stacked); Cys813 (π-alkyl); Cys813 (π-alkyl); Cys813 (π-sulfur); Ile816 (π-σ)	13	-8.4	-0.34	0.68
	Hydrogen bonds	Ala339 (carbon-hydrogen) Val341 (carbon-hydrogen) Leu796 (carbon-hydrogen)				
14	Hydrophobic interactions	Asn138 (halogen); Leu141 (π-σ); Leu141 (alkyl); Ala335 (π-alkyl); Val338 (π-alkyl); Ala339 (π-alkyl); Ala339 (π-σ); Leu796; (π-alkyl); Tyr799 (π-π stacked); Cys813 (π-sulfur); Cys813 (π-alkyl); Ile816 (π-σ);	16	-9.2	-0.33	0.18
	Hydrogen bonds	Asn138 (carbon-hydrogen) Ala339 (carbon-hydrogen) Leu796 (carbon-hydrogen) Cys813 (conventional)				
15	Hydrophobic interactions	Leu141 (π-σ); Ala335 (π-alkyl); Ala335 (π-alkyl); Ala339 (π-alkyl); Ala339 (alkyl); Tyr799 (π-π stacked); Leu796 (alkyl); Cys813 (π-sulfur); Ile816 (alkyl);	10	-8.3	-0.27	0.81
	Hydrogen bonds	Asn138 (conventional)				
16	Hydrophobic interactions	Leu141 (π-σ); Leu141 (alkyl); Ala335 (π-alkyl); Val338 (π-alkyl); Ala339 (π-σ); Ala339 (π-alkyl); Tyr799 (π-π stacked); Cys813 (π-alkyl); Cys813 (alkyl); Ile816 (π-alkyl);	13	-8.4	-0.28	0.68
	Hydrogen bonds	Ala339; (carbon-hydrogen) Val341; (carbon-hydrogen) Glu343 (carbon-hydrogen)				
17	Hydrophobic interactions	Leu141 (π-σ); Ala335 (π-alkyl); Val338 (π-alkyl); Ala339 (π-σ); Ala339 (π-alkyl); Tyr799 (π-π stacked); Cys813 (π-sulfur); Ile816 (π-σ);	12	-9.5	-0.35	0.11
	Hydrogen bonds	Val341 (carbon-hydrogen) Glu343 (carbon-hydrogen) Ala339 (carbon-hydrogen) Leu796 (carbon-hydrogen)				
18	Hydrophobic interactions	Leu141 (π-σ); Leu141 (alkyl); Ala335 (π-alkyl); Ala335 (alkyl); Val338 (alkyl); Ala339 (π-σ); Leu796 (π-alkyl); Tyr799 (π-π T-shaped); Cys813 (π-alkyl); Ile816 (π-alkyl);	10	-8.5	-0.33	0.58
19	Hydrophobic interactions	Tyr799 (π-alkyl); Cys813 (alkyl);	2	-7.7	-0.24	2.24

20	Hydrophobic interactions	Leu141 (π-σ); Ala335 (π-alkyl); Ala335 (π-alkyl); Ala335 (halogen); Ala339 (π-alkyl); Tyr799 (π-π stacked); Leu811 (halogen); Cys813 (π-sulfur); Cys813 (alkyl); Ile816 (π-alkyl); Ile816 (alkyl);	12	-9.5	-0.34	0.11
	Hydrogen bonds	Asn138 (conventional);				
21	Hydrophobic interactions	Leu141 (π-σ); Ala335 (π-alkyl); Val338 (π-alkyl); Ala339 (π-σ); Ala339 (π-alkyl); Tyr799 (π-π stacked); Cys813 (π-sulfur); Cys813 (π-alkyl); Ile816 (π-σ);	10	-9.8	-0.39	0.06
	Hydrogen bonds	Leu796 (carbon-hydrogen);				
22	Hydrophobic interactions	Leu141 (π-σ); Leu141 (alkyl); Ala335 (π-alkyl); Val338 (π-alkyl); Ala339 (π-σ); Ala339 (π-alkyl); Tyr799 (π-π stacked); Cys813 (π-sulfur); Cys813 (π-alkyl); Ile816 (π-σ);	12	-9.0	-0.38	0.25
	Hydrogen bonds	Glu343 (conventional); Leu796 (carbon-hydrogen);				
23	Hydrophobic interactions	Leu141 (π-alkyl); Ala335 (π-σ); Ala339 (halogen); Ala339 (halogen); Ala339 (π-alkyl); Ala339 (alkyl); Glu343 (halogen); Glu343 (halogen); Tyr799 (π-π T-shaped); Tyr799 (π-π T-shaped); Cys813 (π-sulfur); Cys813 (π-alkyl); Ile816 ((π-σ); Ile816 (alkyl);	15	-9.3	-0.34	0.15
	Hydrogen bonds	Asn138 (conventional);				
24	Hydrophobic interactions	Asn138 (halogen); Leu141 (alkyl); Ala335 (π- alkyl); Ala339 (π-alkyl); Ala339 (alkyl); Tyr799 (π-π T-shaped); Ile816 (alkyl);	9	-8.3	-0.28	0.81
	Hydrogen bonds	Tyr799 (conventional); Leu811 (conventional);				
25	Hydrophobic interactions	Leu141 (π-alkyl); Ala335 (π-σ); Ala339 (π-alkyl); Ala339 (alkyl); Tyr799 (π-π T-shaped); Tyr799 (π-alkyl); Cys813 (π-σ); Ile816 (π-σ);	9	-10.2	-0.35	0.03
	Hydrogen bonds	Asn138 (conventional);				
26	Hydrophobic interactions	Leu141 (π-σ); Ala335 (π-alkyl); Val338 (π-alkyl); Ala339 (π-σ); Tyr799 (π-π stacked); Cys813 (π-sulfur); Cys813 (π-alkyl); Ile816 (π-alkyl);	8	-9.0	-0.34	0.25
27	Hydrophobic Interactions	Asn138 (halogen); Leu141 (alkyl); Val331 (π-alkyl); Ala335 (π-alkyl); Ala339 (π-alkyl); Ala339 (alkyl); Tyr799 (π-π T-shaped); Ile816 (alkyl);	10	-8.1	-0.26	1.14
	Hydrogen bonds	Asn138 (conventional); Tyr799 (conventional);				

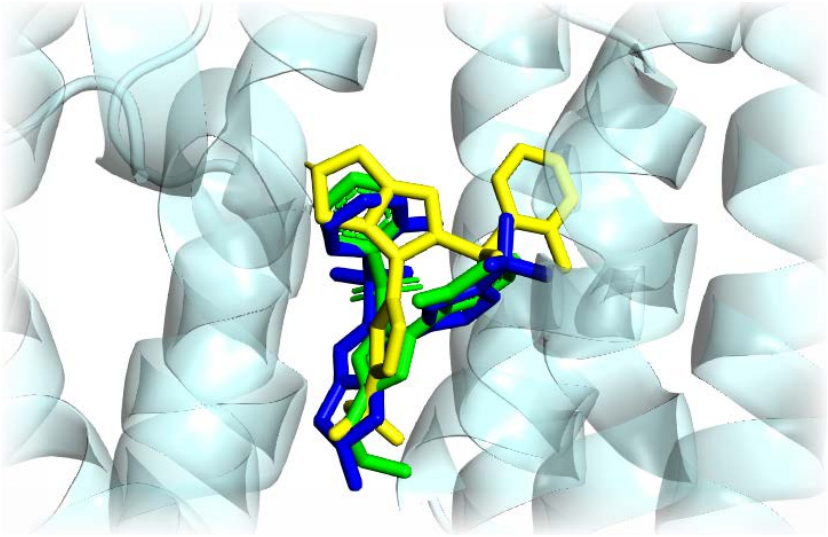

Figure 16. *Mutual binding orientation of vonoprazan (colored green) and the best-docked conformations of compounds 14 (colored blue) and 23 (colored yellow) in the active site of the gastric proton pump*.

Considering all binding parameters data, it can be concluded that derivatives 14 and 23 formed the highest number of significant binding interactions with simultaneously low values of the achieved docking scores. The binding orientation of these two compounds with respect to binding mode of vonoprazan in the active site of gastric proton pump is shown in Figure 16.

DISCUSSION

The aim of this *in silico* study was to design vonoprazan derivatives using a specific distribution-based approach to obtain molecules with optimized physico-chemical properties that can accumulate in the acidic environment of the stomach. The initial set of drawn compounds consisted of 40 molecules, of which 27 compounds were selected for further molecular docking analysis based on the applied drug-likeness filter. Binding potential of the selected vonoprazan derivatives was assessed using molecular docking study to identify the derivatives with the highest binding affinity to the gastric proton pump. The crystal structure of the gastric proton pump with PDB code 5YLU was selected for molecular docking analysis. Binding mode analogy was determined by comparing the molecular docking of vonoprazan and investigated compounds into the structure of targeted ATPase. Within the binding analysis, category, type, total number of significant binding non-covalent interactions, docking score, ligand efficiency parameter, and inhibition constants were determined.

In the present *in silico* study we performed the optimization of psysico-chemical properties (pK_a and $logD_{7.4}$) to obtain new molecules with improved absorption and increased distribution in the stomach. As a model, we used the structure of the lipophilic base vonoprazan with a pK_a of 9.1 - 9.3 and a $logD_{7.4}$ of 0.4 in blood (19, 38). The calculated pK_a values of our tested compounds ranged from 3.66 to 6.66, indicating that our compounds are weaker bases than vonoprazan. Based on the predicted percentage of the ionized form of molecule at pH = 1 (approximately 99%), we can conclude that these compounds are predominantly present in their ionic state in the stomach, so they are ion-trapped in this acidic environment. Moreover, the investigated molecules exhibited a $logD_{7.4}$ values in the range from 1.84 to 2.82, which is optimal for gastrointestinal absorption (39). In addition, the absorption data obtained using the BOILED-Egg and pkCSM predictive model indicated that designed compounds have a very high degree of gastrointestinal absorption.

The values of the obtained docking scores revealed that 9 compounds, derivatives 1, 6, 11, 14, 17, 20, 21, 23, and 25 had lower binding energies

compared to vonoprazan, while derivatives 12, 22, and 26 had the same binding score as vonoprazan (-9.0 kcal/mol). Compounds 11, 21 and 25 were characterized by the lowest achieved binding energy of -9.7, -9.8 and -10.2 kcal/mol, respectively. The lower value of the estimated free binding energy and the inhibition constant indicate a stronger interaction between tested compound and the proton gastric pump. In comparison, similar *in silico* study performed by Muh'd and co-workers showed that the investigated quinazolinone derivatives achieved comparable docking scores ranging from -9.3 to -7.2 kcal/mol (40). Noor and associates performed a molecular docking evaluation of benzimidazole-pyrazole hybrids in AutoDock Vina, thereby the investigated compounds showed similar values of docking scores (-9.8 to -9.0 kcal/mol) as designed compounds (-10.2 to -7.4 kcal/mol) (41). On the other hand, Wang and co-workers designed the molecule SH-337, using very similar distribution-based approach as in our study. Molecule SH-337 had a $logD_{7.4}$ value of 1.3 and a pK_a of 9.0 and demonstrated the significantly lower value of docking score (-11.53 kcal/mol) compared to the tested compounds (20).

The calculated inhibition constants of tested compounds were in the range from 0.03 to 3.71 μM. Namely, derivatives 11, 21, and 25 had the lowest micromolar values of inhibition constant during molecular docking into the active sites of the gastric proton pump (0.08, 0.06, and 0.03 μM, respectively), which were significantly lower than inhibition constant of vonoprazan (0.249 μM).

Since molecular masses and number of heavy atoms of tested compounds were in the range from 358.39 to 453.49 g/mol and 24 to 31 atoms, the ligand efficiency parameter was chosen as a more precise criterion for ranking the obtained docking scores. Taking into the count the actual potency of a compound with respect to the molecular size, ligand efficiency introduced by Andrews (42) can be a useful parameter in the leading compound selection (43). It is obvious that molecules that achieved the given potency with less heavy atoms are more efficient and have lower ligand efficiency values. Based on the calculated ligand efficiency values, the tested compounds were divided into two groups. The first group consisted of derivatives 2, 3, 11, 12, 13, 14, 17, 18, 20, 21, 22, 23, 25, and 26. The ligand efficiency values calculated for these derivatives were between -0.39 and -0,33 kcal/mol/atom, indicating that these derivatives should have higher inhibitory potential towards gastric proton pump than the derivatives in the second group (1, 4, 5, 6, 7, 8, 9, 10, 15, 16, 19, 24, and 27) whose ligand efficiency values ranged from -0.33 to -0.26 kcal/mol/atom. The lowest ligand efficiency value was calculated for compounds 21 and 22 (-0.39 and -0.38 kcal/mol/atom), which is comparable to the ligand efficiency value calculated for vonoprazan (24 heavy atoms, LE = 0.375). The main reason for the higher ligand efficiency values of our tested compounds compared with vonoprazan (except for derivatives 21 and 22) was their slightly different binding orientation in the active site of the gastric proton pump compared with vonoprazan.

During molecular docking of the co-crystallized ligand vonoprazan, a polar non-covalent interaction is formed between the nitrogen atom in its side chain (hydrogen bond donor) and the residue ALA339. In addition, pyridine and phenyl moiety of vonoprazan form multiple hydrophobic contacts with residues ASN138, LEU141, ALA335, VAL338, VAL341, GLU343, LEU796, TYR799, LEU811, CYS813, and ILE816 (12). In the present study, we defined significant binding interactions as those contacts formed by vonoprazan during its molecular docking into the active site of the proton pump.

If we consider the significant binding interactions of our tested compounds, we can highlight derivatives 3, 13, 14, 16, 17, 20, 22 and 23, as those forming the highest number of the significant binding interactions in the active site of the gastric proton pump. The interaction of tested compounds with gastric proton pump is characterized by the formation of multiple π-alkyl interactions with residues ALA335, ALA339 and ILE816, with the thiophene and pyridine rings usually involved in the formation of these hydrophobic interactions. It has been also noted that tested compounds with their pyridine, thiophene, phenyl, and fused nitrogen heterocyclic rings form different types of interactions with residue CYS813 (π-sulfur and π-alkyl). The thiophene core of compound 3 (Figure 8), the phenyl moiety of compound 20 (Figure 13), and the pyridine ring of derivative 13, 14, 17, and 20 establish a hydrophobic π-π interaction with residue TYR799 (Figures 9, 10, 12, and 13), whereas pyridine core and fused nitrogen heterocycle of compound 23 form a double π-π contact with the aforementioned amino acid. As for the halogen interactions, the trifluoromethyl group of compound 23 establishes even four

interactions with residues ALA339 and GLU343 (Figure 15). The formation of weak carbon-hydrogen bonds also contributes significantly to the affinity of the tested compounds for the gastric proton pump. Derivatives 13, 14, and 16 each formed three interactions of this type with residues ASN138, GLU344, ALA339, VAL341, and LEU796 (Figures 9-11), while derivative 17 formed four interactions with the aforementioned residues (Figure 12). The formation of strong conventional hydrogen bonds is observed during molecular docking of derivative 14 (CF3 group acts as a hydrogen bond acceptor in interaction with CYS813) (Figure 10), 20 (pyrazole core acts as a hydrogen bond acceptor in interaction with ASN138) (Figure 13), 22 (tertiary nitrogen atom of compound's heterocycle acts as a hydrogen bond donor in interaction with GLU343) (Figure 14), 23 (pyridine ring acts as a hydrogen bond acceptor in interaction with ASN138) (Figure 15) and 25 (pyridine ring acts as a hydrogen bond acceptor in interaction with ASN138) (Figure 7C) into the active site of gastric proton pump. It is obvious that the presence of hydrogen-bonded ASN138 has a great importance for the binding affinity of the tested compounds towards the H^+, K^+-ATPase, resulting in the low value of the docking score, as in the case of derivatives 11 (-9.7 kcal/mol), 20 (-9.5 kcal/mol), 23 (-9.3 kcal/mol), and 25 (-10.2 kcal/mol). On the other hand, it can be observed that the presence of a trifluoromethyl group on benzene nucleus (derivatives 11 and 25) and especially on the thiophene ring (derivatives 14, 20, and 23) leads to lower free binding energy values of -9.7, -10.2, -9.2, -9.5 and -9.3 kcal/mol, respectively. This obtained *in silico* result can be explained by the formation of additional interactions between this group of tested compound and various amino acid residues, in particular derivative 11 with ILE816 (alkyl) and CYS813 (alkyl) (Figure 7A), derivative 14 with ASN138 (C-H hydrogen bond and halogen interaction) (Figure 10), derivative 20 with LEU811 (halogen interaction) (Figure 13), derivative 23 with GLU343 (halogen interaction), ALA339 (halogen and alkyl interaction), and ILE816 (alkyl interaction) (Figure 15), as well as derivative 25 with TYR799 (π-alkyl) and ALA339 (alkyl interaction) (Figure 7C). High values of docking scores of derivatives 17 (-9.5 kcal/mol) and 21 (-9.8 kcal/mol) can be explained by the formation of additional binding interactions originating from the o-tolyl group of the tested compound's side chain. Namely, this aromatic ring docked to the active site of the gastric proton pump and contributed significantly to the stabilization of the ligand-protein complex by forming the additional interactions with LEU141 (π-σ), ALA335 (π-alkyl), VAL338 (π-alkyl), and CYS813 (π-sulfur) (Figures 7B and 12). In the aforementioned study of Wang and co-workers (20), the pyrrole derivative SH-337 demonstrated very similar binding orientation compared to our tested compounds. Namely, nitrogen atom of the aliphatic amine formed two donor hydrogen bonds with carbonyl oxygen atoms of residues GLU795 and GLU343.

Of all tested compounds, derivative 25 showed the lowest value of the docking score (-10.2 kcal/mol). This finding can be clarified by the formation of a grid of hydrophobic interactions between pyridine, phenyl and fused heterocycle of tested compounds and various amino acid residues. Additional stabilization of ligand-protein complex is achieved by the formation of hydrophobic and halogen interactions with the trifluoromethyl group, whereas pyridine ring forms strong polar interaction (hydrogen bond acceptor) with ASN138 residue (hydrogen bond donor).

The main limitation of conducted *in silico* study represents the lack of target protein flexibility. This type of semi-flexible docking protocol provides flexibility of ligand, while the protein residues remain conformationally rigid. Most current docking tools allow limited or no flexibility of the target protein, primarily because of calculation complexity that increases the time required for binding analysis.

CONCLUSION

According to the docking scores obtained in AutoDock Vina, derivatives 11, 21, and 25 showed the highest binding affinity to H^+, K^+-ATPase. However, compounds 3, 13, 14, 16, 17, 20, 22, and 23 formed the highest number of significant binding interactions with the amino acid residues of the gastric proton pump active site. Considering these two parameters simultaneously with ligand efficiency data and calculated inhibition constants, it can be concluded that derivatives 14 and 23 achieved the highest number of significant binding interactions (16 and 15, respectively) with concomitant lower values the docking scores (-9.2 and -9.3 kcal/mol) compared with vonoprazan as a binding control. Thus, based on the binding assessment criteria, these two compounds are molecules with

the strongest inhibitory potential against H^+, K^+-ATPase. In a line with that, derivatives 14 and 23 can be highlighted as the best *in silico* hits for the gastric proton pump inhibition and represent the most promising candidates for further *in vitro* and *in vivo* investigation of their potential in the reduction of gastric acid secretion.

Acknowledgements

This study was approved and financially supported by the Faculty of Medical Sciences, University of Kragujevac.

Conflict of interest

Authors have no conflicts of interest to declare.

References

1. Inatomi N, Matsukawa J, Sakurai Y, et al. Potassium-competitive acid blockers: Advanced therapeutic option for acid-related diseases. Pharmacol Ther 2016;168:12-22. https://doi.org/10.1016/j.pharmthera.2016.08.001

2. Oshima T, Miwa H. Potent Potassium-competitive Acid Blockers: A New Era for the Treatment of Acid-related Diseases. J Neurogastroenterol Motil 2018;24(3):334-44. https://doi.org/10.5056/jnm18029

3. Barocelli E, Ballabeni V. Histamine in the control of gastric acid secretion: a topic review. Pharmacol Res 2003;47(4):299-304. https://doi.org/10.1016/S1043-6618(03)00009-4

4. Sachs G, Shin JM, Howden CW. Review article: the clinical pharmacology of proton pump inhibitors. Aliment Pharmacol Ther 2006;23(2):2-8. https://doi.org/10.1111/j.1365-2036.2006.02943.x

5. Castellana C, Pecere S, Furnari M, et al. Side effects of long-term use of proton pump inhibitors: practical considerations. Pol Arch Intern Med 2021;131(6):541-9. https://doi.org/10.20452/pamw.15997

6. Son M, Park IS, Kim S, et al. Novel Potassium-Competitive Acid Blocker, Tegoprazan, Protects Against Colitis by Improving Gut Barrier Function. Front Immunol 2022;13: 870817. https://doi.org/10.3389/fimmu.2022.870817

7. Hunt RH, Scarpignato C. Potassium-Competitive Acid Blockers (P-CABs): Are They Finally Ready for Prime Time in Acid-Related Disease? Clin Transl Gastroenterol 2015;6(10):e119. https://doi.org/10.1038/ctg.2015.39

8. Shin JM, Cho YM, Sachs G. Chemistry of covalent inhibition of the gastric (H+, K+)-ATPase by proton pump inhibitors. J Am Chem Soc 2004;126(25):7800-11. https://doi.org/10.1021/ja049607w

9. Strand DS, Kim D, Peura DA. 25 Years of Proton Pump Inhibitors: A Comprehensive Review. Gut Liver 2017;11(1):27-37.

https://doi.org/10.5009/gnl15502

10. Chey WD, Mody RR, Izat E. Patient and physician satisfaction with proton pump inhibitors (PPIs): are there opportunities for improvement? Dig Dis Sci 2010;55(12):3415-22. https://doi.org/10.1007/s10620-010-1209-2

11. Tanaka S, Morita M, Yamagishi T, et al. Structural Basis for Binding of Potassium-Competitive Acid Blockers to the Gastric Proton Pump. J Med Chem 2022;65(11):7843-53. https://doi.org/10.1021/acs.jmedchem.2c00338

12. Abe K, Irie K, Nakanishi H, et al. Crystal structures of the gastric proton pump. Nature 2018;556(7700):214-8. https://doi.org/10.1038/s41586-018-0003-8

13. Abe K, Yamamoto K, Irie K, et al. Gastric proton pump with two occluded K+ engineered with sodium pump-mimetic mutations. Nat Commun 2021;12(1):5709. https://doi.org/10.1038/s41467-021-26024-1

14. Lee JS, Cho JY, Song H, et al. Revaprazan, a novel acid pump antagonist, exerts anti-inflammatory action against Helicobacter pylori-induced COX-2 expression by inactivating Akt signaling. J Clin Biochem Nutr 2012;51(2):77-83. https://doi.org/10.3164/jcbn.11-94

15. Garnock-Jones KP. Vonoprazan: first global approval. Drugs 2015;75(4):439-43. https://doi.org/10.1007/s40265-015-0368-z

16. Sugano K. Vonoprazan fumarate, a novel potassium-competitive acid blocker, in the management of gastroesophageal reflux disease: safety and clinical evidence to date. Therap Adv Gastroenterol 2018;11:1756283X17745776. https://doi.org/10.1177/1756283X17745776

17. Takahashi N, Take Y. Tegoprazan, a Novel Potassium-Competitive Acid Blocker to Control Gastric Acid Secretion and Motility. J Pharmacol Exp Ther 2018;364(2):275-86. https://doi.org/10.1124/jpet.117.244202

18. Akazawa Y, Fukuda D, Fukuda Y. Vonoprazan-based therapy for Helicobacter pylori eradication: experience and clinical evidence. Therap Adv Gastroenterol 2016;9(6):845-52. https://doi.org/10.1177/1756283X16668093

19. Otake K, Sakurai Y, Nishida H, et al. Characteristics of the Novel Potassium-Competitive Acid Blocker Vonoprazan Fumarate (TAK-438). Adv Ther 2016;33(7):1140-57. https://doi.org/10.1007/s12325-016-0345-2

20. Wang MS, Gong Y, Zhuo LS et al. Distribution- and Metabolism-Based Drug Discovery: A Potassium-Competitive Acid Blocker as a Proof of Concept. Research (Wash D C) 2022;2022:9852518. https://doi.org/10.34133/2022/9852518

21. Veselinović J, Veselinović A, Toropov A, et al. Monte Carlo method based QSAR modeling of coumarin derivates as potent HIV-1 integrase inhibitors and molecular docking studies of selected 4-phenyl hydroxycoumarins. Acta Fac Med Naiss 2014; 31: 95-103. https://doi.org/10.2478/afmnai-2014-0011

22. Veselinović A, Nikolić G. Protein-protein interaction networks and protein-ligand docking: Contemporary insights and future perspectives. Acta Fac Med Naiss 2021; 38: 5-17. https://doi.org/10.5937/afmnai38-28322

23. Sabe VT, Ntombela T, Jhamba LA, et al. Current trends in computer aided drug design and a highlight of drugs discovered via computational techniques: A review. Eur J Med Chem 2021; 224: 113705. https://doi.org/10.1016/j.ejmech.2021.113705

24. Marvinsketch, 20107. DISPLAYING and characterizing chemical structures, substructures, and reactions, Marvin 17.1.2. ChemAxon. http://www.chemaxon.com

25. Daina A, Michielin O, Zoete V. SwissADME: a free web tool to evaluate pharmacokinetics, drug-likeness and medicinal chemistry friendliness of small molecules. Sci Rep 2017;7(1):1-13. https://doi.org/10.1038/srep42717

26. Lipinski CA, Lombardo F, Dominy BW, et al. Experimental and computational approaches to estimate solubility and permeability in drug

discovery and development settings. Adv Drug Deliv Rev 2001;46:3-26.
https://doi.org/10.1016/s0169-409x(00)00129-0

27. Ghose AK, Viswanadhan VN, Wendoloski JJ. Prediction of Hydrophobic (Lipophilic) Properties of Small Organic Molecules Using Fragmental Methods: An Analysis of ALOGP and CLOGP Methods. J Phys Chem A 1998;102:3762-72.
https://doi.org/10.1021/jp980230o

28. Egan WJ, Merz Jr KM, Baldwin JJ. Prediction of drug absorption using multivariate statistics. J Med Chem 2000;43:3867-77.
https://doi.org/10.1021/jm000292e

29. Veber DF, Johnson SR, Cheng HY, et al. Molecular properties that influence the oral bioavailability of drug candidates. J Med Chem 2002;45:2615-23.
https://doi.org/10.1021/jm020017n

30. Muegge I, Heald SL, Brittelli D. Simple selection criteria for drug-like chemical matter. J Med Chem 2001;44:1841-6.
https://doi.org/10.1021/jm015507e

31. Daina A, Zoete V. A BOILED-Egg To Predict Gastrointestinal Absorption and Brain Penetration of Small Molecules. Chem Med Chem 2016;11:117–21.
https://doi.org/10.1002/cmdc.201600182

32. Pires DE, Blundell TL, Ascher DB. pkCSM: Predicting Small-Molecule Pharmacokinetic and Toxicity Properties Using Graph-Based Signatures. J Med Chem 2015;58(9):4066-72.
https://doi.org/10.1021/acs.jmedchem.5b00104

33. Buntrock RE. ChemOffice Ultra 7.0. J Chem Inf Comput Sci 2002;42(6):1505-6.
https://doi.org/10.1021/ci025575p

34. Morris GM, Huey R, Lindstrom W, et al. AutoDock4 and AutoDockTools4: Automated docking with selective receptor flexibility. J Comput Chem 2009;30(16):2785-91.
https://doi.org/10.1002/jcc.21256

35. Biovia DS, Berman HM, Westbrook J, et al. Dassault Systèmes BIOVIA, Discovery Studio Visualizer, V. 17.2, San Diego: Dassault Systèmes. J Chem Phys 2000;10:21-9991.
Google Scholar

36. Trott O, Olson AJ. AutoDockVina: improving the speed and accuracy of docking with a new scoring function, efficient optimization, and multithreading. J Comput Chem 2010;31 (2):455-61.
https://doi.org/10.1002/jcc.21334

37. Schrödinger L, DeLano W. The PyMOL Molecular Graphics System, Version 2.0 Schrödinger, LLC.
http://www.pymol.org/pymol

38. Nishida H, Arikawa Y, Hirase K, et al. Identification of a novel fluoropyrrole derivative as a potassium-competitive acid blocker with long duration of action. Bioorg Med Chem 2017;25(13):3298-314.
https://doi.org/10.1016/j.bmc.2017.04.014

39. Comer J. High-throughput measurement of log D and pKa. Drug Bioavailability: Estimation of Solubility, Permeability, Absorption and Bioavailability 2003. pp. 21–45.
https://doi.org/10.1002/3527601473.ch2

40. baba Muh'd M, Uzairu, A, Shallangwa, GA, et al. Molecular docking and quantitative structure-activity relationship study of anti-ulcer activity of quinazolinone derivatives. J. King Saud Univ Sci 2020;32(1):657-66.
https://doi.org/10.1016/j.jksus.2018.10.003

41. Noor A, Qazi NG, Nadeem H, et al. Synthesis, characterization, anti-ulcer action and molecular docking evaluation of novel benzimidazole-pyrazole hybrids. Chem Cent J 2017;11(1):85.
https://doi.org/10.1186/s13065-017-0314-0

42. Andrews PR, Craik DJ, Martin JL. Functional group contributions to drug-receptor interactions. J Med Chem 1984;27(12):1648-57.
https://doi.org/10.1021/jm00378a021

43. Hopkins AL, Keserü GM, Leeson PD, et al. The role of ligand efficiency metrics in drug discovery. Nat Rev Drug Discov 2014;13(2):105-21.
https://doi.org/10.1038/nrd4163

Received: March 8, 2023
Revised: September 7, 2023
Accepted: September 15, 2023
Online first: February 2, 2024

Dizajn pirazolskih derivata vonoprazana kao potencijalnih reverzibilnih inhibitora protonske pumpe: *in silico* studija molekularnog dokinga

Marko Karović[1], Boško Nikolić[2], Nikola Nedeljković[1], Marina Vesović[1], Miloš Nikolić[1]

[1]*Univerzitet u Kragujevcu, Fakultet medicinskih nauka, Odsek za farmaciju, Kragujevac, Srbija*
[2]*Univerzitetski klinički centar Kragujevac, Klinika za gastroenterologiju i hepatologiju, Kragujevac, Srbija*

SAŽETAK

Uvod. Uprkos činjenici da se inhibitori protonske pumpe uveliko koriste za inhibiciju lučenja želudačne kiseline, u nedavnim studijama otkriveni su određeni dugoročni neželjeni efekti. Zbog kisele sredine u želucu, veliki je izazov dizajnirati nove kompetitivne inhibitore protonske pumpe sa snažnijom inhibicijom lučenja želudačne kiseline nego kod konvencionalnih lekova.
Cilj rada. Cilj ove *in silico* studije bio je da proceni potencijal odabranih derivata vonoprazana za inhibiciju protonske pumpe primenom studije molekularnog dokinga.
Metode. Dizajn pirazolskih derivata vonoprazana zasnovan na distribuciji sproveden je optimizacijom distributivnog koeficijenta na fiziološkoj pH vrednosti i pKa vrednosti. Studija molekularnog dokinga sprovedena je korišćenjem proteinske strukture protonske pumpe (PDB ID: 5YLU) u kompleksu sa vonoprazanom, u softveru *AutoDock Vina*.
Rezultati. Prema procenjenim vrednostima doking skora, derivati 11, 21 i 25 pokazali su najveći afinitet prema protonskoj pumpi. Jedinjenja 3, 13, 14, 16, 17, 20, 22 i 23 formirala su najveći broj značajnih vezujućih interakcija sa aktivnim mestom protonske pumpe.
Zaključak. Na osnovu dobijenih parametara vezivanja, može se zaključiti da su derivati 14 i 23 postigli najveći broj značajnih vezujućih interakcija (16, odnosno 15), uz istovremeno ostvarene niže vrednosti doking skora (-9,2 i -9,3 kcal/mol), u poređenju sa vonoprazanom kao kontrolom vezivanja. Na osnovu kriterijuma za procenu vezivanja, ova dva jedinjenja predstavljaju molekule sa najsnažnijim inhibitornim potencijalom prema protonskoj pumpi.

Ključne reči: inhibitori protonske pumpe, dizajn zasnovan na distribuciji, derivati vonoprazana, pirazol, molekularni doking